iScience

Article

Efficient radiative cooling based on spectral regulation and atmospheric water harvesting with sunflower design

Graphical abstract

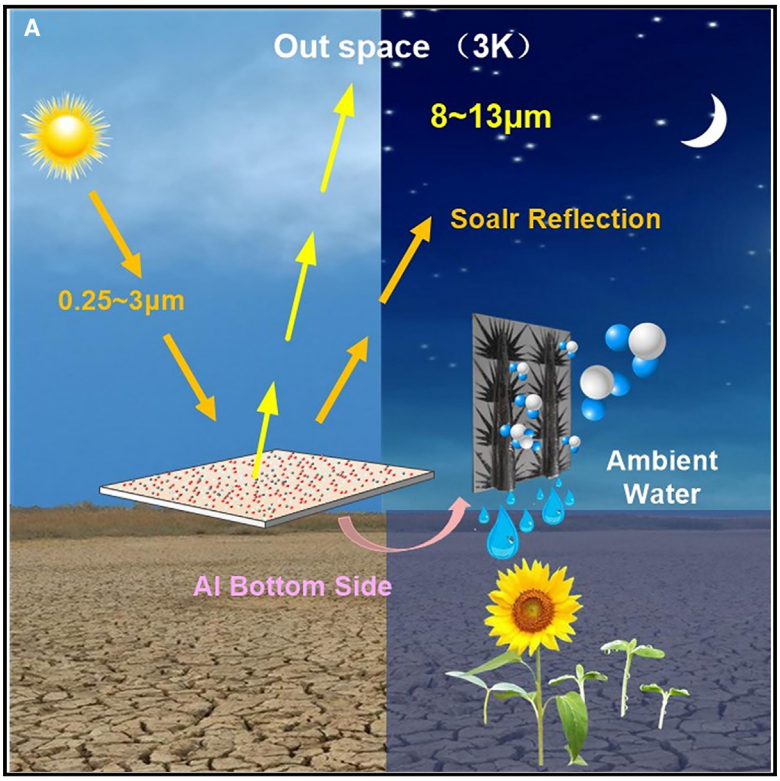

Highlights

- Using nanoparticles to compensate the low peak of PDMS emission spectrum
- The water collection pattern of heterogeneous wettability sunflower was designed
- Enhanced water collection efficiency and droplet directional transport function

Authors

Tao Ma, Jiangbo Wu, Xiaoze Du, Shujun Liu

Correspondence

wujb@lut.edu.cn (J.W.), duxz@ncepu.edu.cn (X.D.)

In brief

Engineering; Materials science; Energy materials

Ma et al., 2025, iScience *28*, 111746
February 21, 2025
https://doi.org/10.1016/j.isci.2025.111746

CellPress

iScience

CellPress
OPEN ACCESS

Article

Efficient radiative cooling based on spectral regulation and atmospheric water harvesting with sunflower design

Tao Ma,[1,3] Jiangbo Wu,[1,3,4,*] Xiaoze Du,[1,2,*] and Shujun Liu[1]

[1]School of Energy and Power Engineering, Lanzhou University of Technology, Lanzhou 730050, China

[2]Key Laboratory of Power Station Energy Transfer Conversion and System of Ministry of Education, North China Electric Power University, Beijing 102206, China

[3]These authors contributed equally

[4]Lead contact

*Correspondence: wujb@lut.edu.cn (J.W.), duxz@ncepu.edu.cn (X.D.)

https://doi.org/10.1016/j.isci.2025.111746

SUMMARY

Inspired by the fog-collecting abilities of the Namib Desert beetle, researchers have developed wettability-engineered surfaces for fog collection. However, these approaches fall short in arid regions where fog is absent. To address these challenges, we developed a dual-sided structure based on radiative cooling. The radiation cooling material on the upper surface can achieve energy free cooling. The lower surface is a pattern with heterogeneous wettability, composed of wedge-shaped and conical structures, which can achieve rapid droplet accumulation and directional transport. The radiation cooling material adjusted by spectrum can achieve a temperature difference of up to 14.2°C, enabling the composite material to achieve a maximum water collection efficiency of 602.5 $g \cdot m^{-2} \cdot h^{-1}$ under RH of 80% conditions. This study provides an effective solution to alleviate water scarcity in arid regions.

INTRODUCTION

The shortage of freshwater resources has always been a global problem, and according to statistics, about 4 billion people are currently suffering from serious water shortages, especially in arid areas.[1–4] To address this global water crisis, desalination and wastewater treatment have emerged as effective solutions.[5,6] However, technical challenges, substantial investment costs, and concerns, such as excessive energy use or ineffective water extraction in arid, low-humidity areas impede the widespread adoption of these methods.[7,8] Since the discovery that the Namib Desert beetle,[9] which borders the Atlantic Ocean, collects moisture in arid environments through its wax-free hydrophilic bumps and wax-coated hydrophobic depressions on its back, several bioinspired materials and water-harvesting systems have been proposed.[10–14] These designs explore the effects of wettability gradients and nanostructure gradients on droplet movement in detail.[15–17] While certain strategies enable the autonomous transport of droplets, the small size of individual water-harvesting units limits their ability to achieve high collection volumes. Micro- and nanoscale structures are difficult to optimize for both droplet accumulation and transportation, requiring larger, more macro-scale structures to achieve significant water collection.[18,19] In addition, many regions are located inland, characterized by arid conditions, and the infrequent occurrence of fog. Even at night, the relative humidity remains low, rendering this fog-harvesting method ineffective in addressing the water scarcity challenges faced by these areas.

In the search for water collection methods tailored to the characteristics of these regions, atmospheric water harvesting (AWH) based on passive daytime radiative cooling (PDRC) has emerged as a promising and viable solution. Reports suggest that approximately 10% of the world's freshwater resources exist as atmospheric water vapor, approximately 12,900 trillion liters of water, 6 times the total volume of the world's rivers, and that substantial amounts of water vapor are present in the atmosphere, even in arid areas such as deserts and mountains.[20,21] The AWH based on PDRC[22–24] uses cooling materials to emit infrared radiation into low-temperature outer space (3 K) through a transparent window (8–13 μm) to cool the material surface from ambient temperature to dew point temperature, thereby condensing and collecting moisture in the atmosphere.[25–27] The principle is shown in Figure 1.

In the study of AWH based on PDRC, Xu[28] investigated the synergistic effect of light-transmitting radiatively cooled membranes to enable a hybrid water cooler to reduce the temperature of condensate during the daytime, with an eventual all-day water production of up to 3654 g $m^{-2} \cdot day^{-1}$, i.e., 152.25 g $m^{-2} \cdot h^{-1}$. Al-Khaya[29] mimicked the structure of the desert beetle dorsal bulge to prepare a heterogeneous wettability pattern, and the highest final water collection of 78 g $m^{-2} \cdot h^{-1}$was obtained at an RH of 95%, an ambient temperature of 22°C, and a post-cooling temperature of 10°C. Xi[30] investigated atmospheric water

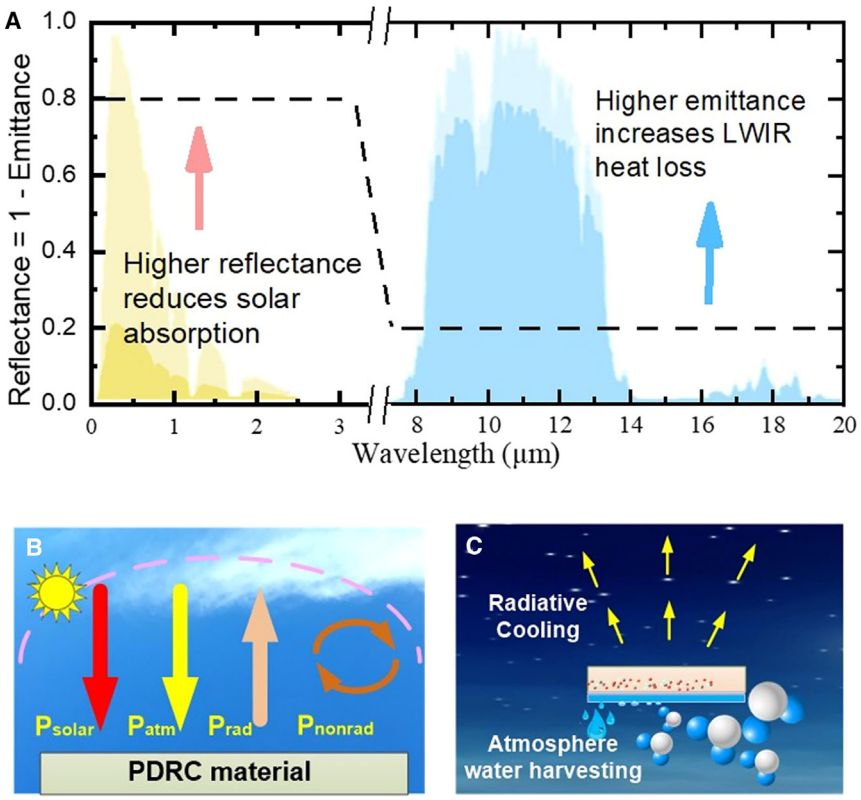

Figure 1. The relevant schematic diagram of the technical principles of PDRC and AWH

(A) The solar spectrum and atmospheric window spectrum.

(B) Schematic diagram of radiation cooling technology.

(C) Schematic diagram of AWH based on PDRC.

harvesting based on radiative cooling during night time and the results showed that the water collection rate was 44 g $m^{-2}\cdot h^{-1}$. Li[31] investigated air water harvesting using low temperature provided by radiative cooling during night time. The results showed that when the RH was 95% and the temperature difference between the ambient temperature and the cooling plate was 10°C, the highest water collection rate of 46.4 g $m^{-2}\cdot h^{-1}$ was finally obtained. It is evident that current atmospheric water harvesting systems based on radiative cooling suffer from low collection efficiency and limited water yield. Moreover, there has been relatively little exploration of their applicability in arid regions with low relative humidity.

Here, based on the inspiration of bionic, we have designed four patterns with high water collection efficiency and directional droplet transportation function for the water collection side of PDRC-AWH by simple spraying method, which are wedge, tree, sunflower, and crown. Each pattern consists of a wedge shape with a 10° tip angle to create a Laplace pressure difference, which, combined with a hydrophilic half-cone handle, strongly enhances the droplet collection rate. In addition, by incorporating dielectric nanomaterials, we adjusted the low emissivity of the radiative cooling material PDMS, enabling a maximum nighttime temperature drop of 14.2°C. This cooling effect allows the material to reach the dew point in Gansu's arid regions during nighttime conditions (ambient temperature of 20°C–25°C, RH 50%–80%), providing a low-temperature guarantee for the water collection side. Ultimately, experimental results demonstrated that, under an ambient temperature of 24°C and RH of 80%, the sunflower achieved the highest condensation rate, reaching 602.5 g $m^{-2}\cdot h^{-1}$. This method offers a feasible solution for water collection in arid, low-humidity regions.

RESULTS

Fabrication

This study presents a passive radiative cooling structure featuring heterowetting. Figure 2A details the fabrication process. Initially, a 4 cm × 4 cm × 0.5 mm Al sheet substrate is ultrasonically cleaned and air-dried for subsequent use. Next, nanoparticles are mixed in alcohol at a predefined ratio and volume fraction, homogenized for 15 min with an ultrasonic homogenizer, and evenly sprayed onto the Al plate. After the alcohol evaporates, the Al plate is positioned on a film scraper. PDMS colloid is applied to a thickness of 150 μm, cured in a 100°C oven for 1 h, and then cooled to room temperature. The substrate is then turned over and sprayed with a pattern with a heterogeneous wetting design. Finally, the material is heated in a 180°C oven for 5 min to finalize the preparation. Figure 2B displays an SEM image of the final radiative cooling material.

Passive radiative cooling

PDMS exhibits remarkable infrared emissivity within the atmospheric window bands. However, its emissivity encounters troughs at the 8∼8.5, 10.5∼11.7, and 12.3∼13 μm wavelengths, which diminishes the overall average emissivity of the material. Si_3N_4, Al_2O_3, and ZnO, possessing strong emissivity within these specific PDMS trough regions, can be utilized to compensate for these deficiencies. By incorporating nanoparticles of Si_3N_4, Al_2O_3, and ZnO, which provide complementary emissive properties, it is possible to adjust the emissivity troughs of PDMS and enhance the overall emissivity of the film. In the experiment, nanoparticles of 50 nm diameter were mixed into 150 μm-thick PDMS at mass fractions of 1%, 3%, and 5%, and the emissivity was tested (results shown in Figure 3A). The findings indicated that the addition of these nanoparticles effectively elevated the emissivity troughs of PDMS, but the emissivity did not increase linearly with higher nanoparticle concentrations. Instead, the overall emissivity reached its peak when the mass fraction of all three nanoparticles was at 3%, achieving an average emissivity of 94.15%, which is a 7.59% improvement over pure PDMS.

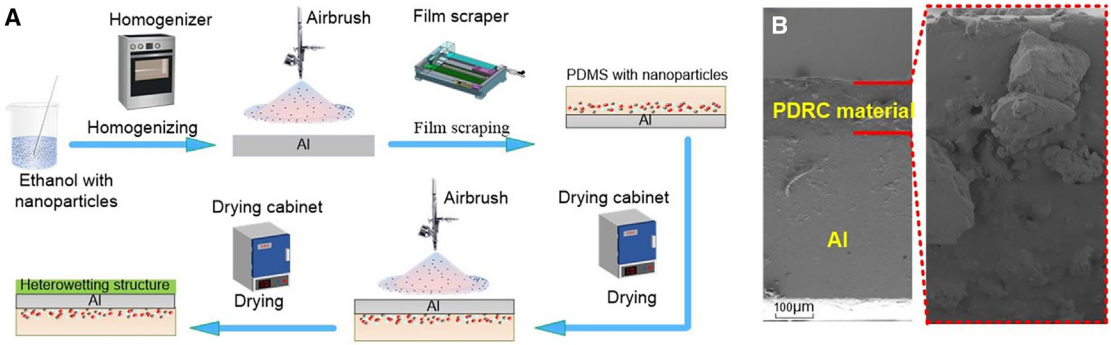

Figure 2. Preparation of the proposed atmospheric water collection material based on radiative cooling

(A) Schematic of the material preparation process.

(B) SEM image of the radiative cooling material.

This lack of a linear correlation is attributed to the fact that while the nanoparticles help to adjust the emissivity troughs, PDMS naturally exhibits higher emissivity in other spectral bands, causing excessive nanoparticle incorporation to diminish the overall emissivity. In addition, incorporating an Al sheet with 94% reflectance as a substrate is essential for achieving solar reflection. This can enhance the cooling effect of the material (see Figure 3B). Figure 3C presents a schematic of the outdoor experimental setup. The device was covered with 400 μm thick polyethylene film to minimize convective heat transfer and air conduction, with its exterior encased in foam boards insulated with cotton.

Figure 3D depicts the temperature reduction achieved through outdoor radiative cooling during daytime and nighttime, respectively. The experimental results show that, on August 17th, a clear day in summer, PDRC could lower the temperature of the covered object by up to 20.6°C under direct sunlight. And on clear nights, the proposed cooling material could lower the base surface temperature by as much as 14.2°C below the ambient temperature. In summary, the cooling effect of radiative cooling materials is superior. The RH of the ambient and solar irradiance during the experiment is shown in Figure 3E. The cooling effect of radiation cooling will provide low-temperature conditions for atmospheric water collection work. Subsequent experiments will focus on studying the effects of different temperature, humidity, and wind speed conditions on the water collection efficiency of different patterns under this temperature drop, as well as achieving the function of moving liquid titration on materials. Considering the unstable outdoor weather conditions, excessive wind speed and rainy or cloudy days can greatly cause experimental errors. Therefore, the subsequent water collection experiment will be completed in a temperature and humidity control box.

Collecting droplets using hetero-wettability sunflower-like structures

The atmospheric water harvesting mechanism, combined with passive radiation cooling, is illustrated in Figures 4A and 4B. On the basis of the low temperature conditions provided by radiation cooling, the surface temperature of the material reaches the dew point temperature, causing water vapor in the atmosphere to condense, thereby achieving atmospheric water harvesting based on radiation cooling. Figure 4C depicts the dew point temperature under different environmental temperatures and relative humidities. From the figure, it is evident that relative humidity has a significant impact on the dew point; under the same conditions, the higher the RH, the higher the dew point temperature, making moisture condensation easier. Gansu is an arid region of northwest China, with rolling hills and little water (see Figure 4D). Nighttime temperatures typically range from 18°C to 25°C during summer and fall, with RH between 50% and 80%. Under such conditions, a temperature difference of 12°C between the cooling material and the ambient air is sufficient for the material's surface to reach the dew point, thus causing condensation of atmospheric moisture. However, for subsequent atmospheric water harvesting, a well-designed structure and heterogeneous wettability arrangement will greatly influence the water harvesting efficiency of the material.

Namib beetles[32] can expedite the condensation and collection of atmospheric moisture more swiftly by virtue of the hetero-structured wettability of their elytral sheaths. Spider silk exploits spindle knots and heterogeneity of joints to drive directional movement of water droplets,[27] akin to how cactus spines direct water from the tip to the base.[33] These phenomena fundamentally rely on the surface free energy gradient[34] and the Laplace pressure gradient,[35] enabling directional liquid transport.

Wedge and cone geometries are traditional designs for directional water collection. A Laplace pressure gradient, which serves as the driving force, enables directional droplet transport. On the wedge, the droplet transport state will vary from 1 to 3 processes (Figure 4E). In states 1 and 2, the droplet stretches and is propelled by the Laplace pressure, until it halts in state 3. Equation 1 calculates the Laplace pressure difference throughout this process.

$$P_1 \sim \gamma_{lg}/R_1, P_2 \sim \gamma_{lg}/R_2$$
$$\Delta P \sim \gamma_{lg}(1/R_1 - 1/R_2) > 0 \quad \text{(Equation 1)}$$

where γ_{lg} is the liquid-gas interface tension and P_1 and P_2 are the Laplace pressures at the tip and base, respectively. ΔP

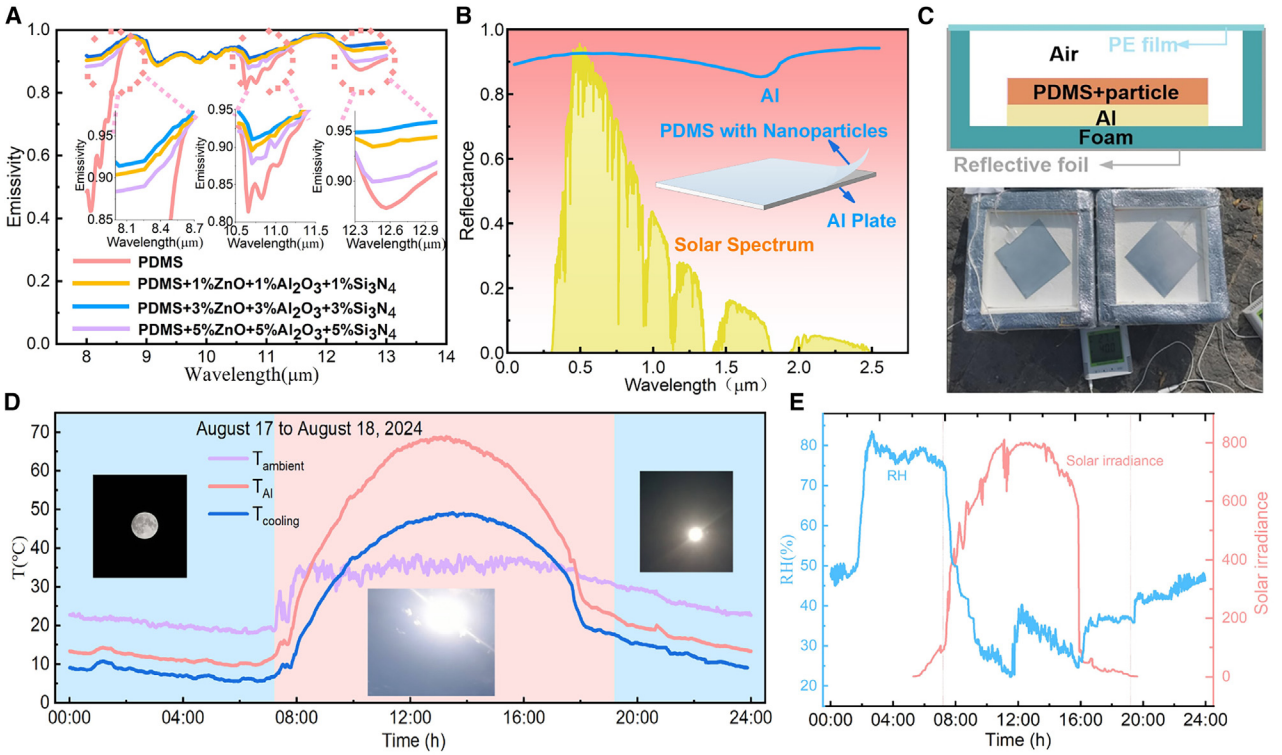

Figure 3. Performance of the radiative cooling material cooling

(A) Impact of different mass fractions of mixed nanoparticles on the emissivity of the PDMS.

(B) Reflectance of Al in the solar radiation wavelength range.

(C) Experimental setup for outdoor radiative cooling tests.

(D) Outdoor PDRC experiments.

(E) Ambient relative humidity and solar irradiance during the experiment.

represents the Laplace pressure difference between P_1 and P_2. This process occurs when $R_1 > R_2$ and persists until the droplet reaches state 3, where it stops.

The curvature gradient of the conical shape generates a Laplace pressure difference affecting the water droplet, as expressed in Equation 2 (Figure 4E).

$$\Delta P = -\int_{R_2}^{R_1} \frac{2\gamma}{(R+R_0)^2} \sin\beta dz \qquad \text{(Equation 2)}$$

where R is the local radius, R_0 is the droplet radius, β is the half vertex angle, and z is the integral variable along the diameter at the tip. The Laplace pressure difference induced by the geometric shape is fundamentally, because R_1 is less than R_2, the Laplace pressure in the high-curvature region (R_1) is greater than the Laplace pressure in the low-curvature region (R_2). This imbalance in the internal Laplace pressure drives the transport of the droplet from the tip to the tail.

To maximize the condensation rate, the developed design incorporates a wedge-shaped pattern that is effective in creating a Laplace pressure difference. Initially, condensation experiments were conducted using base patterns with varying wedge angles to assess the impact of the wedge angle on the droplet transport rate. In these experiments, the wedges were hydrophilic, while their surroundings were coated with a hydrophobic material. The hydrophilic angle was measured to be 75.38°, and the hydrophobic angle was 145.37°, as depicted in Figure 4F.

Finding an optimal wedge tip angle is essential to avoid both excessively large angles, which could cause droplets to prematurely transition into the "free state", and excessively small angles, which could reduce the driving force because of the minimal difference between R_1 and R_2. Accordingly, experiments with tip angles of 5°, 10°, and 15° were conducted to observe the droplet movement over 25 s, as shown in Figure 4G. The experimental results show that for droplets of identical size, a 15° tip angle results in the fastest initial movement, and a 5° tip angle leads to the quickest movement during the middle stage, whereas in the final stage, droplets are accelerated and travel the farthest distance with a 10° tip angle compared to the other two conditions. These phenomena can be explained as follows. A 15° tip angle initially creates a strong Laplace pressure difference, leading to rapid movement. However, with increasing distance, this large tip angle causes the droplet to prematurely transition into the free state. With a 5° tip angle, the droplet encompasses most of the tip because of the small initial angle, resulting in a minimal difference between R_1 and R_2, a small Laplace pressure difference, and slow initial movement. As the

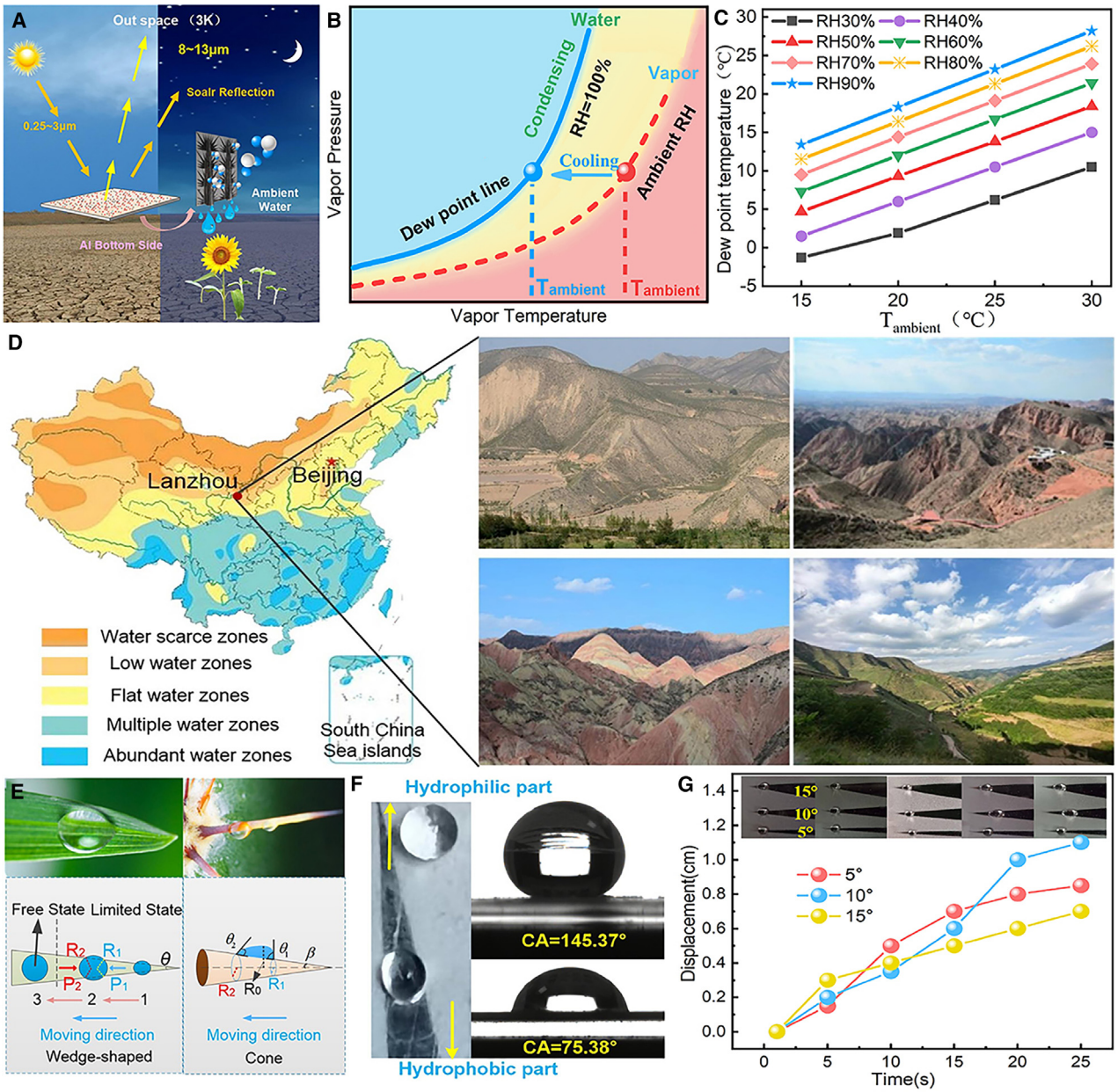

Figure 4. Atmospheric water harvesting technology based on PDRC

(A) Schematic of atmospheric water collection based on radiative cooling.

(B) Cooling and condensation processes of moisture in air.

(C) The corresponding dew point temperature under different ambient temperature and RH.

(D) Landform of Gansu arid area.

(E) Formation of a Laplace pressure gradient.

(F) Heterogeneous wettability contact angles.

(G) Influence of different tip angles on the droplet displacement distance.

droplet travels farther, however, the increasing Laplace pressure difference gradually causes it to accelerate. In contrast, a 10° tip angle ensures consistent displacement, ultimately enabling the droplet to cover the greatest distance. Thus, a 10° tip angle was chosen for the wedge-shaped structures in subsequent designs.

DISCUSSION

After the selection of the 10° wedge-shaped tip angle was finalized, four patterns are designed, which are sunflower shape, crown shape, tree shape, and wedge shape, as shown in Figure 5A. Subsequently, water collection experiments were carried

out on the four patterns. In these models, the regions adorned with patterns exhibit hydrophilicity, while the white areas denote hydrophobicity, as illustrated in Figure 5B. Comparative experiments to assess condensation variations across the patterns were carried out at an ambient temperature of 24°C, with a 14°C temperature difference between the cooling and ambient conditions, and 80% RH, as shown in Figure 5B. The results showed that the sunflower pattern achieved the highest water collection rate of 457.5 g $m^{-2}\cdot h^{-1}$, significantly outperforming others. The crown, tree and wedges pattern followed, with collection rates of 328.5 g $m^{-2}\cdot h^{-1}$, 285 and 178.5 g $m^{-2}\cdot h^{-1}$, respectively. Overall, the water collection efficiency of these heterogeneous wetting patterns is considerable.

Among the four patterns with wedges, the sunflower and crown patterns have higher condensation rates than the wedges and tree patterns because their short, dense wedge distribution provides an effective Laplace pressure difference for droplet movement, which allows for faster and wider water collection, accelerated condensation to form larger droplets, and faster separation. In contrast, the longer wedges in the array's wedge pattern cause more droplets to enter the "free state", which reduces the condensation rate. The water collection rate of the sunflower pattern is superior to that of the crown pattern because of the wider hydrophilic region of the sunflower pattern. In addition, the sunflower pattern also exhibits an instantaneous convergence phenomenon of droplets, as shown in Figure 5C (Video S1), when there are enough tiny droplets on the hydrophilic wedge, it will rapidly shrink and coalesce within a very short time interval (0.03 s), which provides more intuitive evidence for the heightened water-capturing rate of the sunflower pattern, making the sunflower pattern the best choice for water collection.

A hydrophilic half-cone handle was further introduced into the sunflower pattern to facilitate directional droplet transport. This design allows the droplets to move along the handle and disengage at the end of the handle for easier droplet collection. Furthermore, the hydrophilic nature of the handle enhances its ability to capture moisture from the air for condensation, transport, and collection. Figure 5D compares the water collection rates of the sunflower pattern and the version with the added handle. The experiment was performed at an ambient temperature of 24°C and with a 14°C temperature difference between the cooling and ambient conditions. The results show that the water collection rate increases with increasing RH and that the handle-equipped pattern achieves a 24% greater maximum rate than the handle-less sunflower pattern.

In addition, the effect of wind speed on the rate of water harvesting was investigated. The summer wind direction in Northwest of Gansu is mostly from the southeast, and the wind speed is about 1.2–1.7 m/s in most cases on sunny days. Here, the water harvesting experiment results of sunflower patterns with handles were studied under three different wind speeds and relative humidities of 1 m/s, 1.5 m/s, and 2 m/s, as shown in Figure 5E. The results show that in the initial stage (RH = 50%), the smaller the wind speed the highest rate of water collection on the pattern surface. Thereafter, as the RH increases, the water collection rate increases with the wind speed. This is because, under low RH conditions, the higher the wind speed, the easier it is to evaporate the micro droplets on the surface of the water-collecting material, resulting in a lower water-collection rate at high wind speeds. However, with the increase of RH, the high wind speed makes the moisture attach to the water-collecting surface more quickly, which accelerates the water collection. As for the droplet evaporation at high wind speeds, although it will continue, it can no longer cause too much impact under the influence of high humidity and high attachment speeds. Therefore, among the three wind speeds set, the water collection rate will increase as the relative humidity and wind speed continue to increase. And the highest water collection efficiency of 648.5 g $m^{-2}\cdot h^{-1}$was achieved at a wind speed of 2 m/s. Considering the local wind speed factor, the relevant experiments are still carried out at a wind speed of 1.5 m/s in the following experiments.

Figures 5F–5H display the experimental results for different RH and temperature differences, respectively. The experimental results indicate that the water collection rate increases with the increase of relative humidity at a certain temperature difference. Especially when the RH exceeds 70%, the water collection rate significantly increases. When the RH is 80%, the maximum water collection rates under three temperature differences are 351.25, 477.5, and 602.5 g $m^{-2}\cdot h^{-1}$, respectively, indicating a significant enhancement in water collection capacity. Figure 5I compares the water collection rates of the handle-equipped sunflower pattern and the unpatterned Al substrate across varying temperature differentials at RH = 80%. The results show that the water collection efficiency of the sunflower pattern with handle is 3.8 times higher than that of the normal Al plate.

Conclusion

This paper demonstrates a radiative cooling based atmospheric water harvesting effort for efficient cooling and water harvesting transport. We employ nanoparticles to modulate the emission spectrum of PDMS material, the average infrared emissivity is increased by 7.59%. This cooling material can achieve a maximum temperature reduction of 20.6°C on sunny summer days, and at night, the temperature difference can reach up to 14.2°C, providing a low-temperature environment conducive to the condensation of water from the atmosphere. In addition, a sunflower-inspired pattern was designed and combined with heterogeneous wettability to enhance droplet condensation rates and directional transport capabilities. The wedge pattern with a tip angle of 10° maximizes droplet displacement, and the addition of hydrophilic conical handles ensures directional transport of the droplets, achieving a maximum water collection rate of 602.5 g $m^{-2}\cdot h^{-1}$, which is 3.8 times higher than that of ordinary Al plates. Especially at a wind speed of 2 m/s, the sunflower pattern structure with handles significantly improves water collection efficiency, reaching up to 648.5 g $m^{-2}\cdot h^{-1}$. This study provides a feasible solution to alleviate water scarcity in arid regions.

While atmospheric water harvesting via radiative cooling holds promise, it faces several challenges that demand further research. First, climate factors significantly affect the cooling performance of PDRC, as seen from the experimental findings. Cloud cover and high humidity decrease the transparency in the atmospheric window, reducing the cooling efficiency of PDRC. Thus, deploying this technology in high-humidity urban and coastal areas presents challenges, necessitating further

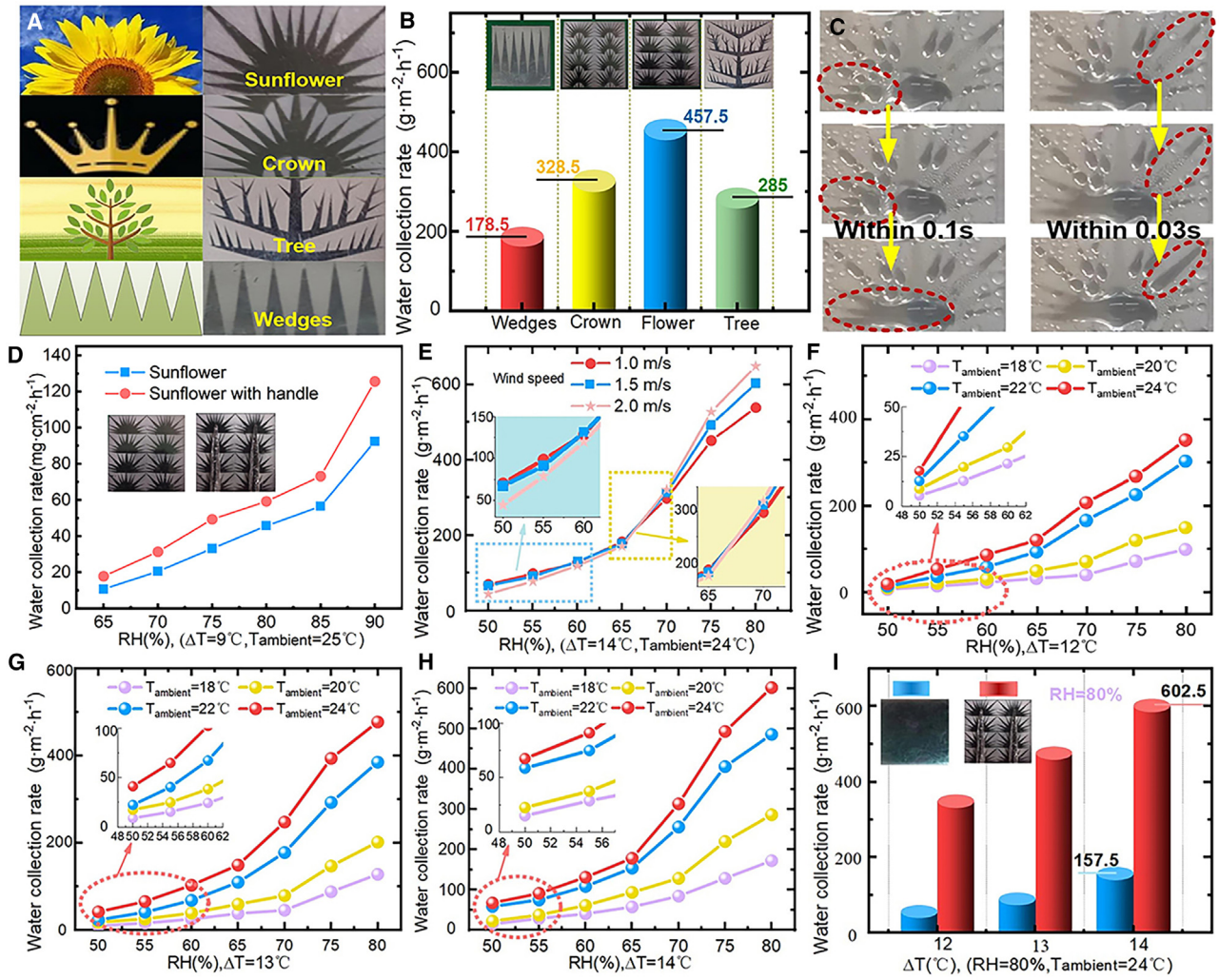

Figure 5. Atmospheric water harvesting performance based on radiative cooling

(A) Different sunflower patterns.

(B) Cooling and condensation processes of moisture in air.

(C) The instant collection of droplets on the surface of a sunflower pattern.

(D) Comparison of water collection rate between sunflower pattern and sunflower pattern after adding handle.

(E) Effect of wind speed on water collection rate.

(F) Water collection rates at a temperature difference of 12°C between the cooling temperature and the environmental temperature.

(G) Water collection rates at a temperature difference of 13°C.

(H) Water collection rates at a temperature difference of 14°C.

(I) Comparison of water collection rates between the sunflower pattern at RH = 80% and an unpatterned Al plate at different temperature differences.

study. Second, the cooling materials used need to maintain physical, optical, and chemical stability. PDRC materials, which are used outdoors, must retain their performance after exposure to wind and sunlight. In addition, an important issue for PDRC materials is that outdoor exposure leads to the accumulation of dust and dirt on their surfaces, which can significantly affect their cooling performance. Consequently, atmospheric water harvesting via radiative cooling presents both many opportunities and many challenges. It also calls for more persistent and collective efforts to develop a sustainable pathway for more efficient air water harvesting in arid regions.

Limitations of the study

Radiative cooling based on atmospheric water collection has certain limitations. First, the high efficiency of PDRC depends on clear weather, cloudy and high humidity weather conditions will reduce the transparency of the atmospheric window, thus affecting the cooling efficiency of PDRC. Secondly, long-term outdoor work may lead to the accumulation of dust and dirt on the surface of the material or affect the physical and chemical stability of the material, and also affect the cooling performance and water collection efficiency of the material.

RESOURCE AVAILABILITY

Lead contact

Requests for further information and resources should be directed to and will be fulfilled by the lead contact, Jiangbo Wu (wujb@lut.edu.cn).

Materials availability

This study did not generate new unique reagents. And all unique/stable reagents generated in this study are available from the lead contact with a completed materials transfer agreement.

Data and code availability

- The data presented in this study are available from the lead contact upon reasonable request.
- This study does not report any original code.
- Any additional information required to reanalyze the data reported in this paper is available from the lead contact upon request.

ACKNOWLEDGMENTS

The authors acknowledge the technical support of the Research Center for Thermal and Fluid Sciences. Thanks to Key Laboratory of Power Station Energy Transfer Conversion and System of Ministry of Education for the equipment help.

Funding: National Natural Science Foundation of China (grant numbers 52130607 and 52366009), Double First-Class Key Program of Gansu Provincial Department of Education (grant number GCJ2022-38), 2022 Gansu Provincial University Industry Support Plan Project (grant number 2022CYZC-21), Key R&D Program of Gansu Province of China (grant number 22YF7GA163).

AUTHOR CONTRIBUTIONS

J.W., X.D., and T.M. conceived and planned this study. T.M. performed the experiment. J.W. and T.M. compiled the material and wrote the manuscript. S.L. conducted a paper check. All authors discussed the results and approved the final version of the manuscript.

DECLARATION OF INTERESTS

The authors declare that they have no competing interest.

STAR★METHODS

Detailed methods are provided in the online version of this paper and include the following:

- KEY RESOURCES TABLE
- METHOD DETAILS
  - Preparation method points to note
  - Passive radiative cooling principles
  - Temperature below the dew point
  - Surface wettability
  - Heat transfer coefficient (HTC)
- QUANTIFICATION AND STATISTICAL ANALYSIS

SUPPLEMENTAL INFORMATION

Supplemental information can be found online at https://doi.org/10.1016/j.isci.2025.111746.

Received: September 30, 2024
Revised: November 7, 2024
Accepted: January 2, 2025
Published: January 4, 2025

REFERENCES

1. Liang, J., Liu, Q., Zhang, H., Li, X., Qian, Z., Lei, M., Li, X., Peng, Y., Li, S., and Zeng, G. (2020). Interactive effects of climate variability and human activities on blue and green water scarcity in rapidly developing watershed. J. Clean. Prod. *265*, 121834. https://doi.org/10.1016/j.jclepro.2020.121834.
2. Salehi, M. (2022). Global water shortage and potable water safety; Today's concern and tomorrow's crisis. Environ. Int. *158*, 106936. https://doi.org/10.1016/j.envint.2021.106936.
3. Huang, X., Mandal, J., Xu, J., and Raman, A.P. (2022). Passive freezing desalination driven by radiative cooling. Joule *6*, 2762–2775. https://doi.org/10.1016/j.joule.2022.10.009.
4. Mekonnen, M.M., and Hoekstra, A.Y. (2016). Four billion people facing severe water scarcity. Sci. Adv. *2*, e1500323. https://doi.org/10.1126/sciadv.1500323.
5. Hao, R., Huang, G., Liu, L., Li, Y., Li, J., and Zhai, M. (2022). Sustainable conjunctive water management model for alleviating water shortage. J. Environ. Manag. *304*, 114243. https://doi.org/10.1016/j.jenvman.2021.114243.
6. Grubert, E.A., Stillwell, A.S., and Webber, M.E. (2014). Where does solar-aided seawater desalination make sense? A method for identifying sustainable sites. Desalination *339*, 10–17. https://doi.org/10.1016/j.desal.2014.02.004.
7. Raveesh, G., Goyal, R., and Tyagi, S.K. (2021). Advances in atmospheric water generation technologies. Energy Convers. Manag. *239*, 114226. https://doi.org/10.1016/j.enconman.2021.114226.
8. Peeters, R., Vanderschaeghe, H., Rongé, J., and Martens, J.A. (2020). Energy performance and climate dependency of technologies for fresh water production from atmospheric water vapour. Environ. Sci. Water Res. Technol. *6*, 2016–2034. https://doi.org/10.1039/d0ew00128g.
9. Parker, A.R., and Lawrence, C.R. (2001). Water capture by a desert beetle. Nature *414*, 33–34. https://doi.org/10.1038/35102108.
10. Yu, Y., Zhang, F., and Yu, H. (2020). Self-healing perovskite solar cells. Sol. Energy *209*, 408–414. https://doi.org/10.1016/j.solener.2020.09.018.
11. Park, J.K., and Kim, S. (2019). Three-dimensionally structured flexible fog harvesting surfaces inspired by Namib Desert Beetles. Micromachines *10*, 201. https://doi.org/10.3390/mi10030201.
12. Yu, Z., Zhang, H., Huang, J., Li, S., Zhang, S., Cheng, Y., Mao, J., Dong, X., Gao, S., Wang, S., et al. (2021). Namib desert beetle inspired special patterned fabric with programmable and gradient wettability for efficient fog harvesting. J. Mater. Sci. Technol. *61*, 85–92. https://doi.org/10.1016/j.jmst.2020.05.054.
13. Liu, M., Peng, Z., Yao, Y., Yang, Y., and Chen, S. (2020). Flexible functional surface for efficient water collection. ACS Appl. Mater. Interfaces *12*, 12256–12263. https://doi.org/10.1021/acsami.9b20222.
14. Park, K.C., Kim, P., Grinthal, A., He, N., Fox, D., Weaver, J.C., and Aizenberg, J. (2016). Condensation on slippery asymmetric bumps. Nature *531*, 78–82. https://doi.org/10.1038/nature16956.
15. Subramanian, R.S., Moumen, N., and McLaughlin, J.B. (2005). Motion of a drop on a solid surface due to a wettability gradient. Langmuir *21*, 11844–11849. https://doi.org/10.1021/la051943i.
16. Zhou, H., Jing, X., and Guo, Z. (2020). Optimal design of a fog collector: unidirectional water transport on a system integrated by conical copper needles with gradient wettability and hydrophilic slippery rough surfaces. Langmuir *36*, 6801–6810. https://doi.org/10.1021/acs.langmuir.0c00987.
17. Daniel, S., Chaudhury, M.K., and Chen, J.C. (2001). Fast drop movements resulting from the phase change on a gradient surface. Science *291*, 633–636. https://doi.org/10.1126/science.291.5504.633.
18. Anand, S., Paxson, A.T., Dhiman, R., Smith, J.D., and Varanasi, K.K. (2012). Enhanced condensation on lubricant-impregnated nanotextured surfaces. ACS Nano *6*, 10122–10129. https://doi.org/10.1021/nn303867y.

19. Wong, T.S., Kang, S.H., Tang, S.K.Y., Smythe, E.J., Hatton, B.D., Grinthal, A., and Aizenberg, J. (2011). Bioinspired self-repairing slippery surfaces with pressure-stable omniphobicity. Nature *477*, 443–447. https://doi.org/10.1038/nature10447.

20. Kim, H., Yang, S., Rao, S.R., Narayanan, S., Kapustin, E.A., Furukawa, H., Umans, A.S., Yaghi, O.M., and Wang, E.N. (2017). Water harvesting from air with metal-organic frameworks powered by natural sunlight. Science *356*, 430–434. https://doi.org/10.1126/science.aam8743.

21. Zhou, X., Lu, H., Zhao, F., and Yu, G. (2020). Atmospheric water harvesting: a review of material and structural designs. ACS Mater. Lett. *2*, 671–684. https://doi.org/10.1021/acsmaterialslett.0c00130.

22. Cheng, Z., Wang, F., Wang, H., Liang, H., and Ma, L. (2019). Effect of embedded polydisperse glass microspheres on radiative cooling of a coating. Int. J. Therm. Science *140*, 358–367. https://doi.org/10.1016/j.ijthermalsci.2019.03.014.

23. Sun, J., Wang, J., Guo, T., Bao, H., and Bai, S. (2022). Daytime passive radiative cooling materials based on disordered media: A review. J. Inflamm. Res. *236*, 111492. https://doi.org/10.1016/j.solmat.2021.111492.

24. Chan, Y.H., Zhang, Y., Tennakoon, T., Fu, S.C., Chan, K.C., Tso, C.Y., Yu, K.M., Wan, M.P., Huang, B.L., Yao, S., et al. (2022). Potential passive cooling methods based on radiation controls in buildings. Energy Convers. Manag. *272*, 116342. https://doi.org/10.1016/j.enconman.2022.116342.

25. Haechler, I., Park, H., Schnoering, G., Gulich, T., Rohner, M., Tripathy, A., Milionis, A., Schutzius, T.M., and Poulikakos, D. (2021). Exploiting radiative cooling for uninterrupted 24-hour water harvesting from the atmosphere. Sci. Adv. *7*, eabf3978. https://doi.org/10.1126/sciadv.abf3978.

26. Wang, Q., Yang, F., Wu, D., and Guo, Z. (2023). Radiative cooling layer boosting hydrophilic-hydrophobic patterned surface for efficient water harvesting. Colloids Surf., A *658*, 130584. https://doi.org/10.1016/j.colsurfa.2022.130584.

27. Zheng, Y., Bai, H., Huang, Z., Tian, X., Nie, F.Q., Zhao, Y., Zhai, J., and Jiang, L. (2010). Directional water collection on wetted spider silk. Nature *463*, 640–643. https://doi.org/10.1038/nature08729.

28. Xu, J., Huo, X., Yan, T., Wang, P., Bai, Z., Chao, J., Yang, R., Wang, R., and Li, T. (2024). All-in-one hybrid atmospheric water harvesting for all-day water production by natural sunlight and radiative cooling. Energy Environ. Sci. *17*, 4988–5001. https://doi.org/10.1039/d3ee04363k.

29. Al-Khayat, O., Hong, J.K., Beck, D.M., Minett, A.I., and Neto, C. (2017). Patterned polymer coatings increase the efficiency of dew harvesting. ACS Appl. Mater. Interfaces *9*, 13676–13684. https://doi.org/10.1021/acsami.6b16248.

30. Xi, Z., Li, S., Yu, L., Yan, H., and Chen, M. (2022). All-day freshwater harvesting by selective solar absorption and radiative cooling. ACS Appl. Mater. Interfaces *14*, 26255–26263. https://doi.org/10.1021/acsami.2c05409.

31. Li, W., Dong, M., Fan, L., John, J.J., Chen, Z., and Fan, S. (2021). Nighttime Radiative Cooling for Water Harvesting from Solar Panels. ACS Photonics *8*, 269–275. https://doi.org/10.1021/acsphotonics.0c01471.

32. Nørgaard, T., and Dacke, M. (2010). Fog-basking behaviour and water collection efficiency in Namib Desert Darkling beetles. Front. Zool. *7*, 1–8. https://doi.org/10.1186/1742-9994-7-23.

33. Ju, J., Bai, H., Zheng, Y., Zhao, T., Fang, R., and Jiang, L. (2012). A multi-structural and multi-functional integrated fog collection system in cactus. Nat. Commun. *3*, 1247. https://doi.org/10.1038/ncomms2253.

34. Chaudhury, M.K., and Whitesides, G.M. (1992). How to make water run uphill. Science *256*, 1539–1541. https://doi.org/10.1126/science.256.5063.1539.

35. Lorenceau, L., and Quéré, D. (2004). Drops on a conical wire. J. Fluid Mech. *510*, 29–45. https://doi.org/10.1017/S0022112004009152.

STAR★METHODS

KEY RESOURCES TABLE

REAGENT or RESOURCE	SOURCE	IDENTIFIER
Chemicals, peptides, and recombinant proteins		
Prepolymer	Hangzhou Weisichuang Technology Co., LTD	CAS:9016-00-6
Fluorosilicon modified silica	Dongguan Zhongke Lingchuang Technology Co., LTD	N/A
Al_2O_3	Beijing Jia Anheng Technology Co., LTD	CAS:1344-28-1
Si_3N_4	Beijing Jia Anheng Technology Co., LTD	CAS:12033-89-5
ZnO	Beijing Jia Anheng Technology Co., LTD	CAS:1314-13-2

METHOD DETAILS

Preparation method points to note

1. When preparing PDMS film, it is necessary to mix prepolymer A and prepolymer B at a ratio of 10:1, and then stir fully for 20min before preparing the film
2. During material preparation, both the radiative cooling side and the atmospheric water harvesting side require spraying techniques. It is crucial to adjust the spray gun's pressure to 4 MPa and maintain a spraying distance of 30 cm from the Al substrate to ensure an even application of nanoparticles and hydrophilic/hydrophobic materials. In addition, when spraying the patterned structures on the water-harvesting side, the template must be securely affixed to the Al substrate to prevent any irregularities in the pattern formation.

This section provides additional information on the derivation of radiation cooling principles, dew point, surface wettability, and heat transfer coefficient.

Passive radiative cooling principles

As an environmentally friendly technology, a radiative emitter can radiate thermal energy to the cold higher sky through atmospheric transparency windows spontaneously. The net cooling power P_{cool} can be calculated by subtracting various heat gains from the atmosphere by radiation (P_{atm}), from the Sun by radiation (P_{sun}), and from the ambient environment through conduction and convection ($P_{cond+conv}$), from the emitted radiative power (P_{rad}). The fundamental equations are listed below, where A is the area, $\int d\Omega = 2\pi \int_0^{\frac{\pi}{2}} d\theta \sin\theta$ is the angular integration over a hemisphere, and $I_{BB}(T,\lambda) = \frac{2hc^2/\lambda^5}{\exp(hc/\lambda K_b T)-1}$ is the spectral radiation of a black body with temperature T. h, K_b, c, and λ are the Planck's constant, the Boltzmann constant, speed of light and wavelength.

Radiation emitted by the cooler:

$$P_{rad}(T) = A\int d\Omega \cos\theta \int_{\lambda=0}^{\infty} I_{BB}(T,\lambda)\varepsilon(\lambda,\theta)d\lambda \quad \text{(Equation 3)}$$

Radiation received from the atmosphere:

$$P_{atm}(T_{amb}) = A\int d\Omega \cos\theta \int_{\lambda=0}^{\infty} I_{BB}(T_{amb},\lambda)\varepsilon_{atm}(\lambda,\theta)\varepsilon(\lambda,\theta)d\lambda \quad \text{(Equation 4)}$$

Radiation received from the Sun:

$$P_{sun} = A\int_{\lambda=0}^{\infty} I_{AM1.5}(\lambda)\varepsilon(\lambda,\theta_{sun})d\lambda \quad \text{(Equation 5)}$$

Heat flux received from the ambient through conduction and convection:

$$P_{cond+conv}(T,T_{amb}) = Ah_c(T_{amb}-T) \quad \text{(Equation 6)}$$

Net cooling power:

$$P_{cool}(T) = P_{rad}(T) - P_{atm}(T_{amb}) - P_{sun} - P_{cond+conv}(T,T_{amb}) \quad \text{(Equation 7)}$$

Cooling power (P_{cool}) and cooling temperature (T_{cool}) are usually the two indexes to evaluate the effectiveness of a cooler. $P_{cool,max}$ is to describe the maximum cooling power at the initial state when there is not yet cooling. T_{cool} is defined as $T_{cool} = T_{amb} - T$ and its maximum ($T_{cool,max}$) is achieved when Pcool reaches its minimum.

The atmosphere has high transmittance for the wavelength of 8–13 μm, and sometimes for 2.5–5, 16–22 μm. 8–13 μm is considered the main atmospheric window because it matches the peak of thermal infrared emitted from the earth's surfaces with a temperature of about 300 K.

Temperature below the dew point

Sub-cooling is the condition where the water vapor has a temperature below its dew point temperature. As shown in Figure 4B, the atmosphere has a low RH in the initial state. To achieve condensation, for a given ambient vapor pressure (i.e., absolute humidity), RH should be increased to reach the saturation condition. A cooling source is necessary for the nearby atmosphere vapor of ambient air temperature to reduce to the corresponding required dew point temperature. As a result, one of the requirements of achieving condensation is the maximum cooling temperature (Tcool,max) should be large enough to reach dew point temperature, i.e. $T_{cool,max} \geq T_{amb}-T_{d.p.} \approx 20 \times (1- RH)$.

Surface wettability

Surface wettability is defined as the tendency of one fluid to spread on or adhere to a solid surface in the presence of other immiscible fluids. Surface wettability, depending on surface chemical compositions and topographic structures, is always characterized by the contact angle, governed by Young's equation $\cos\theta=(\gamma_{sv}-\gamma_{sl})/\gamma_{lv}$, where θ is the contact angle, and γ_{sv}, γ_{sl}, and γ_{lv} are the surface tensions between solid-vapor, solid-liquid, and liquid-vapor, respectively. A surface is classified as hydrophilic when its static contact angle is less than 90°, hydrophobic when it is between 90° and 150°, and superhydrophobic when it exceeds 150°.

Heat transfer coefficient (HTC)

Heat transfer coefficient (HTC) is defined as $h = Q/A/(T_{\infty}-T_s)$, where Q is the heat transfer rate, A is the area, and T_{∞} and T_s are temperatures of water vapor and condensing surface. During condensation heat transfer, the overall heat flux includes the condensation heat flux and sensible heat flux. When the panel was operated with low sub-cooling, the condensation heat flux occupies less than one-third of the overall cooling capacity in buildings with radiative cooling.

QUANTIFICATION AND STATISTICAL ANALYSIS

There are no quantification or statistical analyses to include in this study.